FIELD FLATNESS AND NON-STATIONARY BEHAVIOUR OF THE 4*7-CELL-TESLA-SUPERSTRUCTURE

H.-W. Glock, D. Hecht, U. van Rienen
Institut für Allgemeine Elektrotechnik,Universität Rostock
Albert Einstein-Straße 2, D-18051 Rostock, Germany

Abstract

A structure of four coupled 7-cell resonators has been proposed [1] to increase the effective gradient of TESLA [2]. Each so-called "superstructure" is fed through a single input coupler. The sensitivity of field flatness against geometrical deviations and the time dependence of the fields during fill- and refill-time are studied by means of MAFIA [3] calculations using an optimized grid. The consistency of MAFIA results for perturbed versus unperturbed fields is confirmed utilizing an analytical relation. Non-stationary fields are expanded in a set of eigenmodes calculated with MAFIA. The method is described in some detail and results are presented in comparison with the respective results on the established 9-cell-structure.

1 INTRODUCTION

Overall length is a dominant cost contribution to the total investment for a linear collider. Therefore it is an important task to fill a given length as dense as possible with active, i.e. accelerating, elements. A modified so-called "superstructure" of four coupled 7-cell cavities has been proposed [1] to improve the fill factor of the TESLA [2] accelerator compared to the present design of decoupled 9-cell cavities. Furthermore the superstructure will need only a single input coupler driving the complete string. This paper describes two main aspects of the operation of such a superstructure we are investigating: the question of field flatness sensitivity against shape deviations and the non-stationary behaviour during filling time and beam passage. The following section describes a specialized grid that allows to approximate the cavity shape without staircases of the material distribution. Section 3 contains a method to confirm consistency of MAFIA results on modified boundary shapes. In section 4 the fundamental mode flatness sensitivity against a certain perturbation of a single cell is compared with a similar perturbation of a standard 9-cell resonator. Section 5 gives some detail about the calculation of transients based on eigenmode expansion and shows the results, again in comparison with a 9-cell resonator.

2 GRID GENERATION

A proper discretization of the cavity surface is essential for reliable numerical results, especially if small deviations are to be studied. Therefore the grid has been generated in a special manner: At each point of intersection of a certain r-mesh line with the cavity shape a z-mesh line was placed. Then the boundary is approximated by those mesh cell´s diagonals, which are secants of the curvature. Thus no staircases appear in the material distribution. On the other hand this leads to widely spread mesh cell dimensions, since both very high and very low slopes - corresponding to very narrow and very large z-mesh steps - have to be covered. Therefore the r-mesh positions have to be chosen carefully in a manner, that all given points of the structure were hit exactly, and that the local mesh step ratios are kept in reasonable limits.

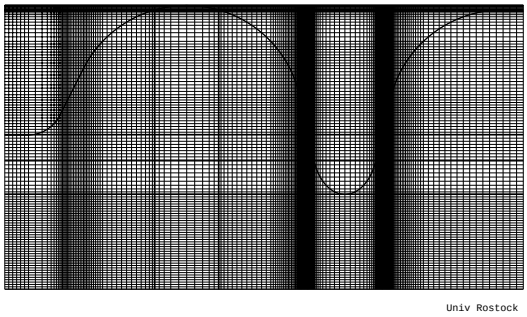

Figure 1: Part of the cavity shape and grid lines. High slopes of the boundary curve lead to dense z-mesh lines, regions of low slopes need dense r-mesh lines.

3 MAFIA CALCULATIONS OF CAVITY SHAPE PERTURBATIONS

In order to confirm the consistency of MAFIA-calculated fields and eigenfrequencies of perturbed and unperturbed cavities we calculated either case directly. Further we used expression (1) which is derived from Maxwell´s equations without any approximation:

$$\omega - \omega_0 = \frac{i \oint\!\!\oint_{\Delta A} \left(\vec{H} \times \vec{E}_0^*\right) d\vec{A}}{\iiint_V \left(\varepsilon \vec{E}\,\vec{E}_0^* + \mu \vec{H}\,\vec{H}_0^*\right) dV} \,. \qquad (1)$$

Herein $(\vec{E}_0, \vec{H}_0, \omega_0)$ stands for the field distribution and eigenfrequency of the unperturbed cavity, $(\vec{E}, \vec{H}, \omega)$ similar of the perturbed one. V is the volume of the perturbed cavity; ΔA the closed surface of the insertion. If this insertion is located at the boundary of the unperturbed volume (like in the case shown in Fig. 2), only the inner part of ΔA contributes to the integral.

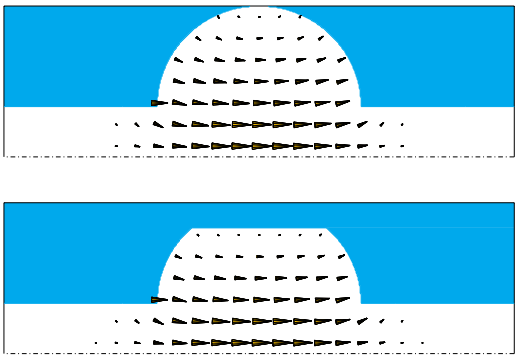

Figure 1: Upper half cross section of model cavity without (upper) and with perturbation. Arrows indicate the fundamental mode E-field, found at 4.3866 GHz (unpert.) and 4.9120 GHz (pert.)

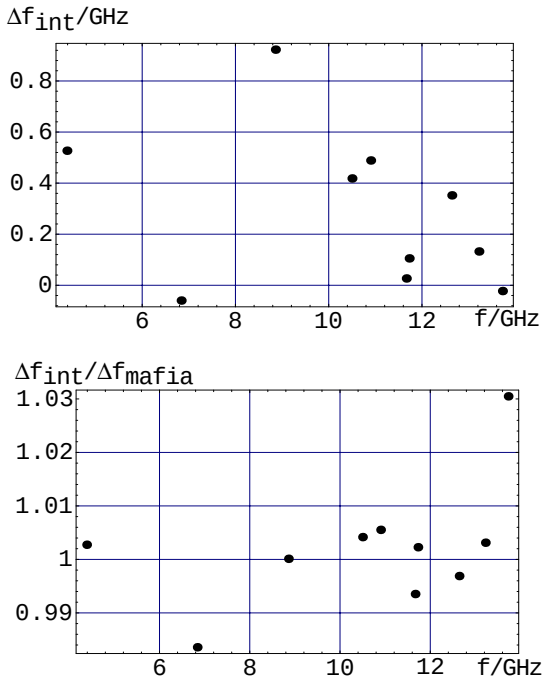

Figure 3 a, b: Frequency deviations Δf_{int} between perturbed and unperturbed cavities calculated from the right hand side fraction of Equ. (1) (upper); ratio of Δf_{int} to the difference of MAFIA-eigenfrequencies for the first 10 modes vs. unperturbed frequency (lower graph).

The consistency of the MAFIA-runs with and without perturbation is confirmed by evaluating Eqn. (1). This has been done in the case of 2D-calculated TM0-Modes. Then the surface integration (numerator) is reduced to a line integral that can be integrated using the MAFIA postprozessor. Some additional effort has to be spent to perform the cross product of the fields which has to be done in the 2D-case in elementary steps. The volume integral in the denominator is calculated abusing the MAFIA energy integration. To do this one has to prepare two extra fields with single components equal to

$$\sqrt{\varepsilon \vec{E} \vec{E}_0^*} \text{ and } \sqrt{\mu \vec{H} \vec{H}_0^*} .$$

Further attention has to be paid to the sign of the square root´s arguments. The result of the right hand side fraction of Equ. (1) is displayed in Fig. 3 normalized to the frequency spread calculated directly for the first 10 modes of the geometry shown in Fig. 2. In general one can observe an agreement within a few percent, mostly below 1%. There is some tendency to smaller errors in case of higher frequency shifts. An unavoidable contribution to the differences comes from the line integral that has to be calculated for technical reasons one mesh line below the surface of the insertion. A second run with doubled distance was made in order to estimate the influence of this effect. Most of the errors were approximately doubled, too, so we asume the reason of the major part of the difference to be caused by the technical difficulty of the testing method.

4 SENSITIVITY OF NORMAL AND SUPERSTRUCTURE

Four cavities are coupled in the superstructure. Therefore it is important to know about the influence of single boundary perturbations on the overall field flatness. In the first cell of the third cavity we applied an insertion at the cell´s equator in a manner shown in Fig. 4. The radius of the cell shrinked from 104.935 mm to 104.53 mm. A similar insertion was applied to a standard 9-cell resonator. In either case this corresponds to a full ring of additional material since the calculations were done in 2D. We observe an unflatness of similar amount. The field disturbance covers a wider range in the long structure which one may judge as it´s disadvantage.

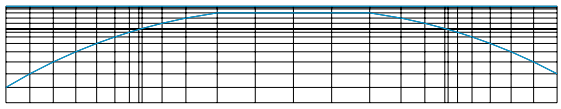

Figure 4: Part of grid and cell boundary with material insertion at the equator.

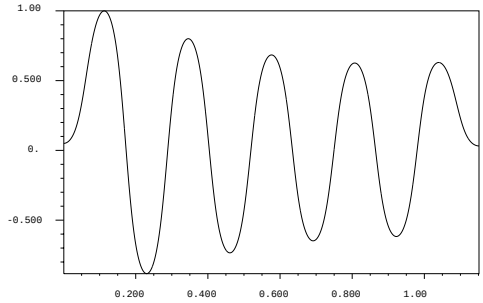

Figure 5: MAFIA-profile of accelerating field in 9-cell resonator with 0.405 mm reduced radius in first cell (cf. Fig. 4).

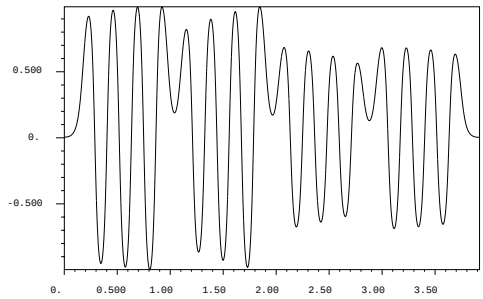

Figure 6: MAFIA-profile of accelerating field in 4x7-cell resonator with 0.405 mm reduced radius in first cell of third resonator (≈ 2.1 m, cf. Fig. 4).

5 FILLING AND BEAM LOADING

Recent developments of input couplers and their power transmission capabilities made it possible to feed a complete superstructure with a single coupler. Then one has to look whether the filling process will be completed in the given time. Further the question arises whether the power taken away by the beam is re-established fast enough in order not to shrink the beam energy gain during the bunch train passage. To calculate this one could think of direct time domain simulation. In fact this is practically impossible for a mesh volume of approximately 450.000 points and a time intervall that covers about 10^6 oscillations. Therefore we used the approach of eigenmode decomposition (e.g. [4], [5]). A similar calculation with slightly different assumptions and based on another code has been done from Ferrario and Sekutowicz ([6], [7]). Our results are in good agreement with theirs.

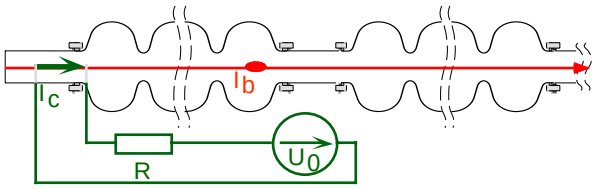

Figure 7: Model used for time domain calculations based on eigenmode expansions.

The model used for the calculation is shown in Fig. 7. The eigenmodes of the resonators are excited by the beam current I_b and a short transmitter driven current path I_c. An ideal rf-source with voltage U_0 together with it´s inner resistance R are used to decribe the transmitter. For reasons of simplicity I_c is placed on axis in the beam pipe near the beginning of the first cell. This is justified by a proportionality factor, common to all modes, of the axis fields to the fields at the real input coupler position. Since external Qs are about 10^4 lower than unloaded ones, resistive losses of the cavities are neglected. So the transmitter resistance is the only damping within the system, that furthermore causes a mode-to-mode coupling. Only the 28 modes of the fundamental passband were taken into account. This is justified by the large frequency gap to the next higher passbands, which appear above 2 GHz.

Starting from Maxwell´s equations we find:

$$-\frac{1}{\mu}\Delta\vec{E}+\varepsilon\,\partial_t^2\vec{E}=-\partial_t\vec{j}\ . \tag{2}$$

The electrical field is expanded in a set of eigenmodes:

$$\vec{E}(\vec{r},t)=\sum_\nu a_\nu(t)\,\frac{\vec{E}_\nu(\vec{r})}{\sqrt{2\,W_\nu}}\ . \tag{3}$$

Each eigenmode solves:

$$\Delta\vec{E}_\nu+k_\nu^2\vec{E}_\nu=0\quad\text{with}\quad k_\nu^2=\omega_\nu^2\,\varepsilon\mu \tag{4}$$

and therefore holds:

$$\varepsilon\sum_\nu\left[\frac{\vec{E}_\nu(\vec{r})}{\sqrt{2\,W_\nu}}\left(\omega_\nu^2+\partial_t^2\right)a_\nu(t)\right]=-\partial_t\vec{j}\ . \tag{5}$$

Applying the orthogonality of the eigenmodes:

$$\iiint_{V_{res}}\varepsilon\,\vec{E}_\xi\,\vec{E}_\zeta\,dV=2\delta_{\xi\zeta}\,W_\zeta \tag{6}$$

yields:

$$\left(\omega_\nu^2+\partial_t^2\right)a_\nu(t)=-\partial_t\,c_\nu(t) \tag{7}$$

with the abbreviation:

$$c_\nu(t):=\iiint_{V_{res}}\frac{\vec{j}(\vec{r},t)\,\vec{E}_\nu(\vec{r})}{\sqrt{2\,W_\nu}}\,dV\ . \tag{8}$$

Equ. (8) gives the expansion coefficients of the currents in the eigenmode system. The total current is splitted in beam (index b) and transmitter driven current (index c):

$$\vec{j}(\vec{r},t)=\vec{j}_b(\vec{r},t)+\vec{j}_c(\vec{r},t) \tag{9}$$

or respectively:

$$c_\nu(t)=c_{\nu,b}(t)+c_{\nu,c}(t)\ . \tag{10}$$

If the beam travels on-axis with constant velocity v the following holds:

$$c_{\nu,b}(t)=\int_{z-axis}\frac{I_b(t-\frac{z}{v})\,\vec{e}_z\,\vec{E}_\nu(\vec{r})}{\sqrt{2\,W_\nu}}\,dz\ . \tag{11}$$

Similarily we get for the transmitter current which is assumed to be constant along it´s path:

$$c_{\nu,c}(t)=I_c(t)\,\frac{\int_{curr.-path}\vec{E}_\nu(\vec{r})\,d\vec{r}}{\sqrt{2\,W_\nu}}=:I_c(t)\,K_\nu\ . \tag{12}$$

Eqn. (12) defines the important abbreviation K_ν that allows to write Kirchhoff´s law along the external circuit:

$$U_c(t)+R\,I_c(t)=U_0(t) \tag{13}$$

as:

$$-\frac{1}{R}\sum_\nu a_\nu(t)\,K_\nu+I_c(t)=\frac{U_0(t)}{R}\ . \tag{14}$$

From (7), (10), (12) and the time derivative of (14) a system of coupled differential equations in the $a_\nu(t)$ follows:

$$\begin{aligned}\left(\omega_\nu^2+\partial_t^2\right)a_\nu(t)+\frac{1}{R}\sum_m K_\nu\,K_m\,\partial_t\,a_\nu(t)=\\=-\partial_t\left[c_{\nu,b}(t)+\frac{K_\nu}{R}\,U_0(t)\right]\quad\forall\,\nu\end{aligned} \tag{15}$$

Introducing a second set of variables:

$$b_\nu := \frac{1}{i\,\omega_\nu}\,\partial_t\,a_\nu \;\Leftrightarrow\; \partial_t\,a_\nu = i\,\omega_\nu\,b_\nu \;\Leftrightarrow\; \partial_t^2\,a_\nu = i\,\omega_\nu\,\partial_t\,b_\nu \tag{16}$$

(the b_ν are the amplitudes of the B-fields) and using an additional abbreviation for the inhomogenity in (15):

$$s_\nu := \frac{i}{\omega_\nu}\,\partial_t\left[c_{\nu,b}(t) + \frac{K_\nu}{R}\,U_0(t)\right] \tag{17}$$

we arrive at a system of differential equations written in matrix-vector-notation:

$$\partial_t\begin{pmatrix} a_1 \\ b_1 \\ \vdots \\ a_n \\ b_n \end{pmatrix} - \begin{pmatrix} 0 & i\,\omega_1 & \cdots & 0 & 0 \\ i\,\omega_1 & -\frac{K_1^2}{R} & \cdots & 0 & -\frac{K_1\,K_n\,\omega_n}{R\,\omega_1} \\ \vdots & \vdots & & \vdots & \vdots \\ 0 & 0 & \cdots & 0 & i\,\omega_n \\ 0 & -\frac{K_n\,K_1\,\omega_1}{R\,\omega_n} & \cdots & i\,\omega_n & -\frac{K_n^2}{R} \end{pmatrix}\begin{pmatrix} a_1 \\ b_1 \\ \vdots \\ a_n \\ b_n \end{pmatrix} = \begin{pmatrix} 0 \\ s_1 \\ \vdots \\ 0 \\ s_n \end{pmatrix} \tag{18}$$

or

$$\partial_t\,\vec{v} - \underline{\underline{M}}\,\vec{v} = \vec{s}\ . \tag{19}$$

The corresponding homogeneous system:

$$\partial_t\,\vec{v} - \underline{\underline{M}}\,\vec{v} = 0 \tag{20}$$

has the well known general solution:

$$\vec{v}(t) = \sum_{j=1}^{2n}\left(\vec{e}_j\,e^{\lambda_j t}\,u_j\right) \tag{21}$$

with the number of modes n used to expand the fields, the eigenvalues λ_j and the eigenvectors $\vec{e}_j$ of $\underline{\underline{M}}$ and arbitrary constants u_j. The calculation of λ_j and $\vec{e}_j$ is done numerically which is (beside the field calculation) the only non-analytical step in the procedure. To solve the inhomogeneous sytem (19) the u_j are assumed to be time dependent. They can be found with some additional steps and by means of Cramer´s rule as:

$$u_j(t) = \frac{\det\left(\vec{e}_1, \ldots, \int_{\tau=0}^{t} e^{-\lambda_j \tau}\,\vec{s}(\tau)\,d\tau, \ldots, \vec{e}_{2n}\right)}{\det\left(\vec{e}_1, \ldots, \vec{e}_{2n}\right)}\ . \tag{22}$$

In (22) the additional assumption was made that all excitations are vanishing before $t = 0$. We´ll refer to the time dependent vector that replaces $\vec{e}_j$ in the numerator determinant as:

$$\int_{\tau=0}^{t} e^{-\lambda_j \tau}\,\vec{s}(\tau)\,d\tau = \vec{W}_j(t) = \vec{W}_{b,j}(t) + \vec{W}_{c,j}(t)\ . \tag{23}$$

Herein the beam excitation is represented by $\vec{W}_{b,j}(t)$, the transmitter current by $\vec{W}_{c,j}(t)$. For all times $t > 0$ we assume a time dependence of the transmitter voltage like:

$$U_0(t) = V_0\,e^{+i\,\omega_0 t} \tag{24}$$

which allows for an explicit integration:

$$\vec{W}_{c,j}(t) = \frac{V_0}{R}\,\vec{K}\,\frac{\omega_0}{i\,\omega_0 - \lambda_j}\left[1 - e^{(i\,\omega_0 - \lambda_j)\,t}\right] \tag{25}$$

$$\text{with } \vec{K} = \begin{pmatrix} \vdots \\ 0 \\ K_\nu / \omega_\nu \\ \vdots \end{pmatrix}. \tag{26}$$

The beam is composed as chain of single charges q, traversing $z = 0$ at different times $t = t_b$ (an additional charge counting index omitted). Thus we have to replace in (11):

$$I_{b,\delta}(t,z) = q\,\delta\left(t - t_b - \frac{z}{v}\right) \tag{27}$$

After some further steps this leads to:

$$\vec{W}_{b,j} = i\,q\,v\,\lambda_j\left(\sum_{t_b < (t - L_{res}/v)} e^{-\lambda_j t_b}\right)\times \times \begin{pmatrix} \vdots \\ 0 \\ \frac{1}{\omega_\nu\sqrt{2\,W_\nu}}\left(\int_{\tau=0}^{L_{res}/v} e^{-\lambda_j \tau}\,E_{z,\nu}(v\,\tau)\,d\tau\right) \\ \vdots \end{pmatrix} \tag{28}$$

In (28) only the sum and the charge depend on beam parameters; all other quantities are determined from the cavity modes. During a charge´s transversal the result of (28) is in error for the contribution of this single charge, which is counted at a whole after the charge left the resonator. The solution of the mode amplitudes searched for is found from Eqns. (21), (22), (23), (25) and (28):

$$\begin{pmatrix} a_1(t) \\ b_1(t) \\ \vdots \\ a_n(t) \\ b_n(t) \end{pmatrix} = \frac{\sum_{j=1}^{2n}\left[\vec{e}_j\,e^{\lambda_j t}\det\left(\vec{e}_1, \cdots, \left(\vec{W}_{b,j}(t) + \vec{W}_{c,j}(t)\right), \cdots, \vec{e}_{2n}\right)\right]}{\det\left(\vec{e}_1, \ldots, \vec{e}_{2n}\right)} \tag{29}$$

The case before a beam transverses the cavity reads as:

$$\begin{pmatrix} a_1(t) \\ b_1(t) \\ \vdots \\ a_n(t) \\ b_n(t) \end{pmatrix} = \frac{V_0\,\omega_0}{R}\,\frac{\sum_{j=1}^{2n}\left[\vec{e}_j\,\frac{e^{\lambda_j t} - e^{i\,\omega_0 t}}{\omega_0 + i\,\lambda_j}\det\left(\vec{e}_1, \ldots, \vec{K}, \ldots, \vec{e}_{2n}\right)\right]}{\det\left(\vec{e}_1, \ldots, \vec{e}_{2n}\right)} \tag{30}$$

In the TESLA scheme 1130 bunches of 5.7267 nC charge are foreseen following each other in a distance of 919 rf periods. The injection of the first bunch happens at rf period 760336 (584.6 μs) at half the unloaded steady state voltage. From this an external Q = 3446120 follows. This data allows to calculate the transmitter resistance, which of course is only valid for a certain coupling, defined by length and position of the current path. For the calculations in Fig. 8 a (slightly to low) Q = 3433810 was found from the $\underline{\underline{M}}$-eigenvalue λ_j according:

$$Q_j = \frac{\omega_j}{2\,\alpha_j} = \frac{\left|\mathrm{Im}\left(\lambda_j\right)\right|}{2\,\mathrm{Re}\left(\lambda_j\right)} \tag{30}$$

This results in a voltage decrease (cf. Tab. 1) during the

bunch train and is cited here to illustrate the dependencies. The voltage was calibrated to be 25 MV/m inside the resonators at first injection, equal to 80.6756 MV in total. This total gradient was investigated for each bunch with an improved Q. The remaining deviations appear as jitter of below ±1000 V (courtesy M. Dohlus).

Ez/(MV/m)	cell 1	cell 7	cell 28
bunch 1	47.352	48.009	47.426
bunch 1130	47.089	47.831	47.044
decrease	-0.55%	-0.37%	-0.80%

Table 1: Decrease of accelerating voltage caused by slight mismatch of transmitter resistance, i.e. coupling.

Fig. 8 shows as the result of our calculations a sequence of field profiles illustrating the process of build-up, profile stabilization and the influence of the beam. Fig. 9 shows a similar picture under same conditions for a 9-cell structure after 10^4 rf periods. As expected, it´s field amplitudes are higher at this time and the flatness is better. Nevertheless the field in the superstructure is obviously established fast enough and the profile with beam remains stable.

6 CONCLUSION AND OUTLOOK

We studied two main aspects of a 4x7-cell "superstructure" in comparison with the standard TESLA-9-cell cavity. Neither the filling and refilling of the superstructure nor the field flatness sensitivity contradict a sucessfull operation. Further studies will target the higher order mode behaviour.

ACKNOWLEDGEMENT AND SUPPORT

The authors wish to thank M. Dohlus, DESY, who had a strong impact on the work presented here.
This work was supported by DESY.

REFERENCES

[1] J. Sekutowicz, M. Ferrario, C. Tang: Superconducting Superstructure; LC97, Sept./Oct. 97, Zvenigorod, Russia
[2] R. Brinkmann, G. Materlik, J. Rossbach, A. Wagner (Eds.): "Conceptual Design of a 500 GeV e^+e^- Linear Collider with Integrated X-ray Laser Facility", DESY 1997-048
[3] MAFIA V. 4.015, CST, D-64289 Darmstadt
[4] M. Dohlus, R. Schuhmann, T. Weiland: "Calculation of frequency Domain Parameters Using 3D Eigensolutions", International Journal of Numerical Modelling: Electronic Networks, Devices and Fields (invited, to be published)
[5] H.-W. Glock, P. Hülsmann, M. Kurz, H. Klein: "Rise Time of Amplitudes of Time Harmonic Fields in Multicell Cavities", Proc. 1993 Particle Accelerator Conference, May 1993, Washington D.C., pp. 623-625
[6] M. Ferrario, A. Mosnier, L. Serafini, F. Tazzioli, J.-M. Tessier, "Multi-Bunch Energy Spread Induced by Beam Loading in a Standing Wave Structure", Part.Acc. 52 (1996), pp. 1-30
[7] J. Sekutowicz, M. Ferrario, C. Tang: "Superconducting Superstructure for the TESLA Collider", TESLA-Report 98-08, DESY, April 1998

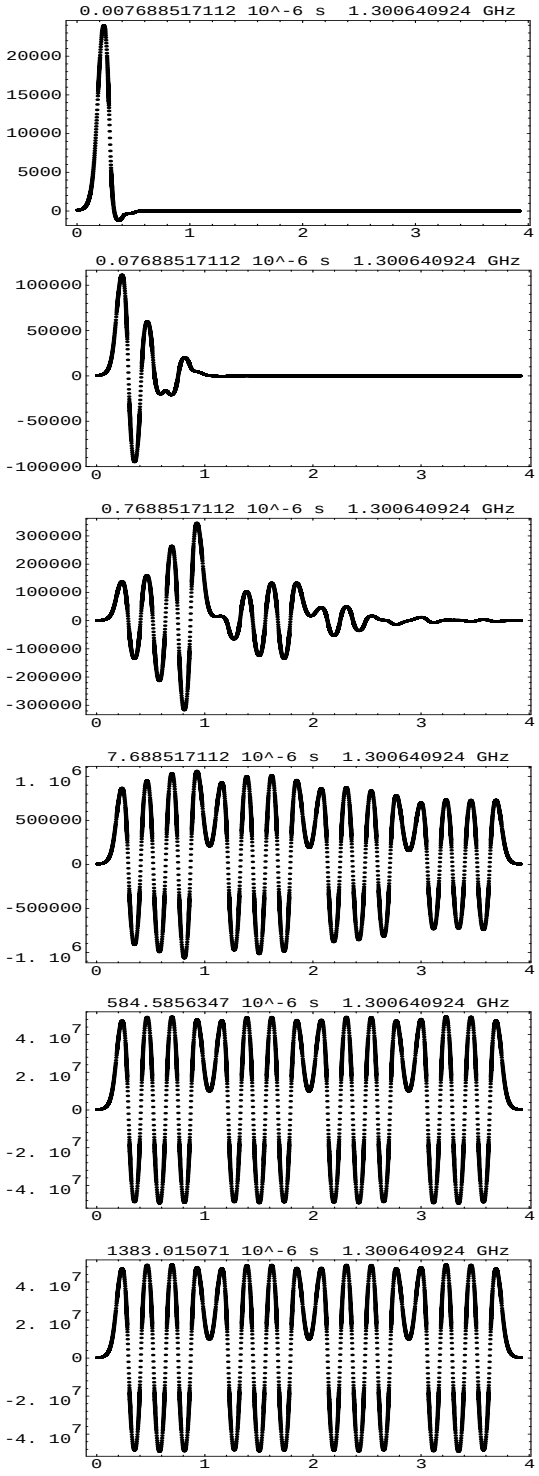

Figure 8: Sequence of field profiles (E_z/(V/m) vs. z/m) at increasing time (10^1 to 10^4 rf periods; first, last bunch)

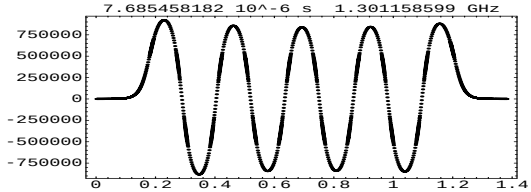

Figure 9: Field profile of 9-cell cavity after 10^4 rf periods; the profile is almost stabilized.